Hindawi
Shock and Vibration
Volume 2018, Article ID 1936560, 16 pages
https://doi.org/10.1155/2018/1936560

Research Article

Dynamic Finite Element Analysis of a New Type Flexible Rock Shed under the Impact of Rock Block and Improving the Design

Lianming Cui,[1] **Min Wang**,[1,2] **and Tangrong Yu**[1]

[1]*Army Logistical University of PLA, Chongqing 401331, China*
[2]*College of Mechanical Engineering, Nanjing University of Science and Technology, Nanjing 210094, China*

Correspondence should be addressed to Min Wang; wangmin198217@163.com

Received 7 June 2018; Accepted 6 August 2018; Published 15 November 2018

Academic Editor: Francesco Franco

A 1:1 flexible rock shed made of flexible nets and steel-vaulted structure is manufactured and tested for functional evaluation with impact experiment previously. To further discuss the performance of this structure under the impact of rockfalls and to improve the design, numerical simulation for this structure is carried out in this paper. Firstly, the simplified numerical models for characterizing the mechanical behavior of the ring nets and wire meshes are deduced. Then, a detailed finite element model for the flexible rock shed is developed for impact analysis. By comparing the experimental data, the numerical model for the flexible rock shed is shown to be reliable in predicting the dynamic behavior of the flexible rock shed. Finally, combined with the numerical simulation results and experimental results, an improved design is presented, and the numerical simulation results show that the energy dispersion in the improved design of the rock shed is more equalized, and damages on the steel-vaulted structure are much improved.

1. Introduction

With transportation construction extended to the western mountain area in China, the rockfall disaster is becoming more and more universal [1]. The reinforced concrete rock shed is widely used for rockfall protection in China and other countries (Figure 1). However, the impact load on these structures is large under the impact of rock block, the volume and the weight of the structures would be increased, and the large deep burial and large section foundation would be needed [2–5]. For these reasons, the construction is usually very difficult and needs increasing the costs. In order to overcome such construction difficulty and to reduce costs, a new type of flexible rock shed is proposed (Figure 2(a)). The structure is mainly composed of steel-vaulted structure (Figure 2(b)) and flexible nets (Figure 2(c)) and is designed to stand for an impact energy of about 250 kJ considering the low-to-medium impact energy of rockfall hazard scenarios [6].

The flexible rock shed mixes the flexible barriers and structural rock sheds, and the protection mode for this structure differs from the flexible barriers but the same as the rock shed. Therefore, this solution possesses the advantages of both the flexible barriers and the concrete rock shed and overcomes some limits on them. It is cheaper than the concrete rock shed with the same energy retention capacity. It is easier to construct and can be quickly installed requiring little equipment. The flexible rock shed relies on the deflection of the flexible nets for energy absorption, and in general case, the flexible nets can absorb more energy though the larger deflection, but the adequate safe distance between the system and the ground must be taken into account in design.

A 1:1 flexible rock shed is manufactured and tested for functional evaluation with an impact experiment a few years ago, and it is shown that the structure can stand for an impact energy of about 250 kJ without observable rupture of the flexible nets or cables and can be put into service again with some maintenance on the steel-vaulted structure [7]. Though full-scale field test is of vital importance in the design process, field test cannot provide detailed information such as energy absorption in

Figure 1: Rock shed with reinforced concrete columns, foundations, and a roof slab.

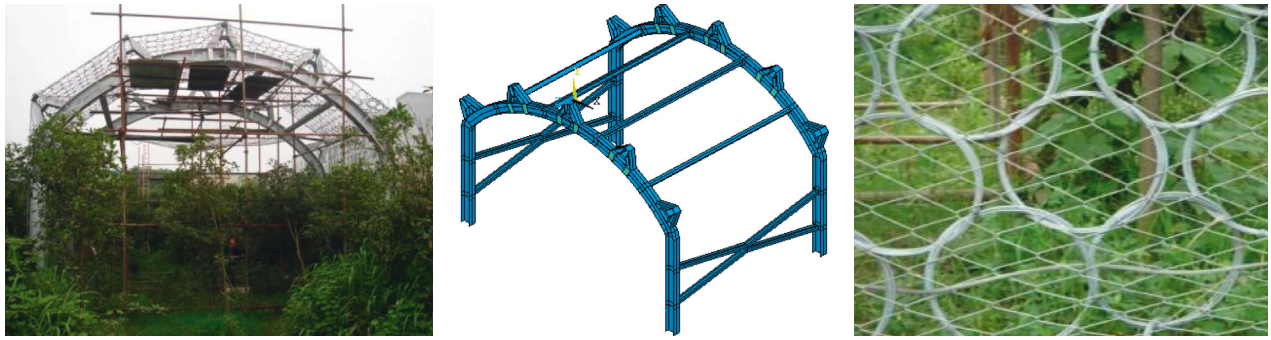

(a) (b) (c)

Figure 2: (a) Flexible rock shed; (b) steel-vaulted structure; (c) ring nets and TECCO wire meshes G65.

individual components and how the support system reacts, which is crucial for improvement of design and enhancement of the performance of the rock shed. In addition, full-scale field tests are time consuming and cost intensive. Alternatively, the application of numerical simulation techniques, especially the finite element method (FEM) or the discrete element method (DEM) and computer-aided design, are becoming essential in the structure analysis.

Flexible rock shed is a complex system with a combination of rockfall barriers and rock shed. With the aim to develop a simplified numerical model for evaluating and improving the performance of the proposed flexible rock shed, a numerical approach is presented by using commercial CAE software package LS-DYNA to simulate impact test of the flexible rock shed. Simulation results are compared with experimental data to assess the accuracy and effectiveness of the proposed numerical approach in predicting the dynamic behavior of the flexible rock shed. In addition, some complementary improvements are made for the structure.

2. A Brief Review of the Experiment

The flexible rock shed (Figure 2(a)) tested is 1:1 model with 8.5 m in span, 5 m in bay, and 7.0 m in height (Figure 3). The steel-vaulted structure is composed of arched beam, the longitudinal supports, the shearing supports, and the net-hanging brackets, and the cross-sectional dimensions of these elements are shown in Table1 and Figure 4.

In the experiment, the quality of rock block is approximately 800 kg, and the shape is 14-face polyhedron (Figure 5). The impact velocity of the block is 25 m/s, and the impact energy of the block is 250 kJ. The impact location is on the middle of the flexible rock shed (Figure 3(b)).

The impact process of the rock block onto the flexible rock shed is recorded by a high-speed camera with 300 frames per second. Dynamical strain gauges are pasted on half of the steel-vaulted structure, and the pasted strain gauges are located at T0, T1-1, T1-2, T1-3, T1-4, and T1-5, as shown in Figure 3(a). Load cells are used for the measurement of tensile force acting on the cable anchors and the horizontal cables (Figure 3(a)).

3. Numerical Approach and Finite Element Model

The flexible rock shed mainly consists of flexible nets and steel-vaulted structure. The flexible nets consist of the ring nets and the wire meshes and are the main energy absorption components. The models to reproduce the highly nonlinear behavior of the ring nets and the wire meshes are one of the key questions in the numerical simulation for the structure and are given in Sections 3.1 and 3.2.

Details about the numerical model of flexible rock shed including element types and material models for each component are given in Section 3.3. Flexible rock shed is a very complex structure with many joints and connections. In Section 3.4, simplifications on connections, impacting condition, and other boundary constraint conditions are also given.

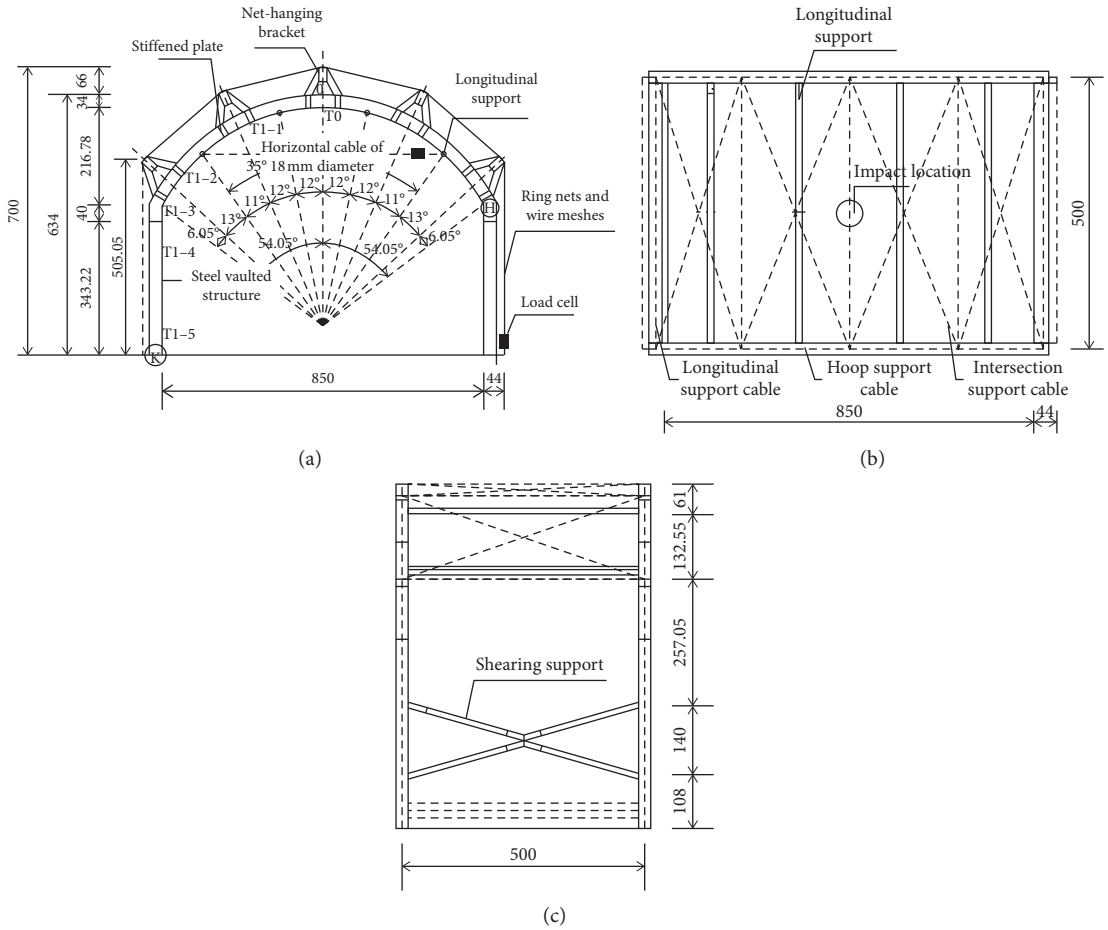

Figure 3: The design of a single-span flexible rock shed. (a) Front view of the designed flexible rock shed; (b) top view of the flexible rock shed; (c) end view of the flexible rock shed.

Table 1: The cross-sectional dimensions of the steel-vaulted structure.

Component	Type (H × B)	Dimension (mm)			Cross section shape
		t1	t2	r	
Arched beam and column	HM340 × 250	9	14	13	
Net-hanging brackets	HM244 × 175	7	11	13	
Longitudinal supports and shearing supports	HM150 × 150	7	10	8	

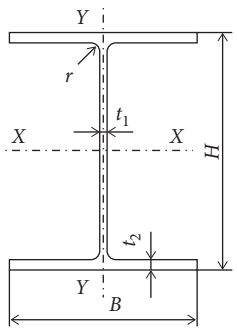

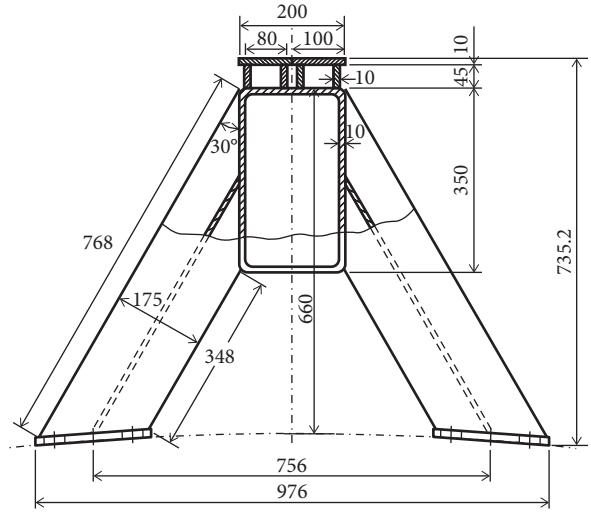

Figure 4: The detailed dimensions of the net-hanging bracket.

3.1. Modeling the Mechanical Behavior of the Ring Nets. The ring nets (Figure 6(a)) are connected by wire ring sets (Figure 6(b)) with a diameter of 300 mm. Each ring set is formed by single wire turned several windings and held together by small clamps, and the wire is made of high strength steel wire with a diameter of 3 mm. In order to simulate the ring nets, it is necessary to analyze and simplify the mechanical analysis of the ring set and establish a numerical model for the ring set firstly. Much

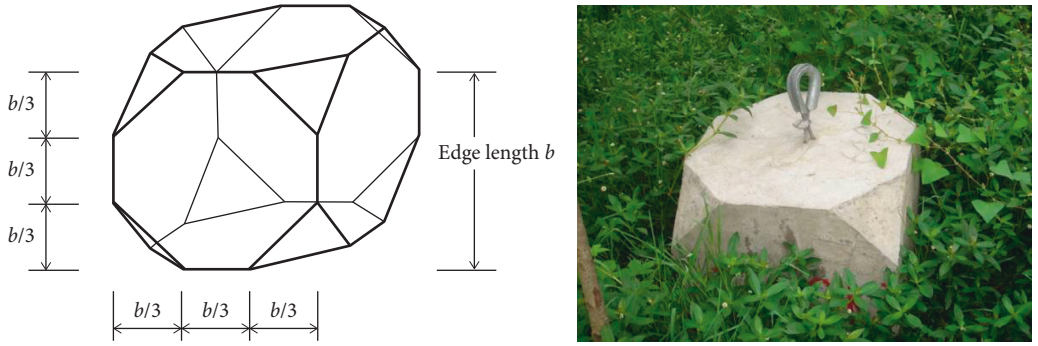

Figure 5: Cubic block of 14-face polyhedron.

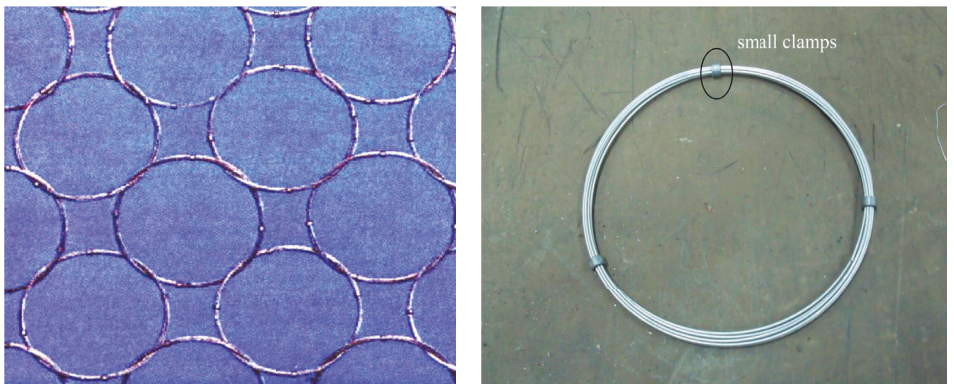

(a) (b)

Figure 6: (a) Ring nets and (b) single ring set.

research has already been carried out to model the ring sets in recent years based on the FEM and DEM methods. With the FEM methods, there are including the model with diagonal springs elements [8] the FEM methods including the model with diagonal elements and linear beam elements in which the inverse formulation is used to calculate the equivalent radius [9]. With the DEM methods, the DEM methods including the model in which the ring sets are discretized into a single node, and the nodes are connected with bar elements [10–12] or innovative discrete model with multicriteria numerical method based on the Levenberg–Marquardt algorithm [13]. In this paper, an analytical formula for calculating the equivalent radius for the circular cross section of ring set is deduced, and the ring set model could be set up in the following.

Lu and Yu [14] investigated the behavior of a single ring with force applied on the two sides (Figure 7). The radius of the single ring is R, the shape of cross section is rectangle, and the cross-sectional height is t ($t \ll R$). Based on a combined effective yield criterion between the cross-sectional bending moment and axial force of the ring,

$$|m| + n^2 = 1, \tag{1}$$

where $m = M/M_0$, $n = N/N_0$, $M_0 = (1/4)\sigma_0 bt^2$, $N_0 = \sigma_0 bt$. M_0 is the limited cross-sectional plastic moment, N_0 is the limited cross-sectional axial force, b is the cross-sectional width, and σ_0 is the cross-sectional yield stress.

The relationship between the tensile force P and the limited cross-sectional axial force N_0 can be deduced by the following approximately balance equation (Figure 7):

$$P = \frac{t}{(1 - \sin\theta)R} N_0. \tag{2}$$

For the ring set formed by steel wire turned several windings, the load can be averaged to each wire ring due to the constraint effect from the clamps. The tensile force and displacement relationship ($P - \delta$ curve) of single wire ring with a radius R and circular cross-sectional radius r ($r \ll R$) can be deduced by the following approximate balance equation:

$$\frac{P}{2} R(1 - \sin\theta) = 2M_p, \tag{3}$$

$$\delta = 2R(\cos\theta + \theta - 1), \tag{4}$$

$$M_p = \frac{4}{3}\sigma_0 r^3, \tag{5}$$

where P is the tensile force, θ is the angle shown in Figure 7, δ is the displacement, M_p is the cross-sectional limited plastic moment, and σ_0 is the cross-sectional yield stress.

Substituting Equation (5) in (3) yields

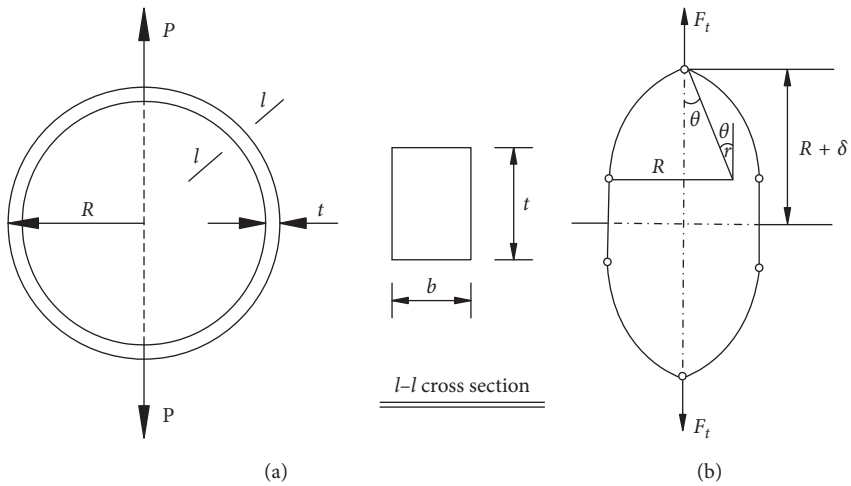

Figure 7: (a) The single ring with the force applied on the two sides. (b) The calculation model for the single ring.

$$\frac{P}{r^3} = \frac{16\sigma_0}{3R(1-\sin\theta)}. \tag{6}$$

Assuming that the ring set consisted of steel wire turned by n windings, if a single wire ring bears load P, the ring set consisted of n wire rings can bear load nP. Assuming the force-displacement curve of a single wire ring is the same as the ring set, consequently, Equation (6) can be rewritten as

$$\frac{nP}{r_1^3} = \frac{16\sigma_0}{3R(1-\sin\theta)}. \tag{7}$$

Hence from Equations (6) and (7), one has

$$\frac{P}{r^3} = \frac{nP}{r_1^3}. \tag{8}$$

So, the equivalent radius of ring set r_1 can be written as

$$r_1 = n^{1/3} r. \tag{9}$$

Figure 8 shows the quasistatic tensile tests for the ring sets by 9 wire rings with force on the two sides, and the experimental force-displacement curves have been described in Figure 9. As a comparison, the analytical force-displacement of the ring set based on the above theory is also presented in Figure 9. Numerical simulation of the tensile test is carried out. The cross section of the ring set is circle, and the equivalent radius is 3.12 mm. The ring set is discretized by beam element, and the model is shown in Figure 10. Geometric and material nonlinearities are considered, and the multilinear isotropic hardening model is used to describe the material behavior. The engineering stress versus strain relationship is obtained by the direct tensile tests on single wire (Figure 11).

The simulation results are also shown in Figure 9. As can be seen in Figure 9, the numerical simulation results coincide well with the theoretical calculation, but the maximum force of numerical simulation results is lower to the tests, and the maximum displacement of the numerical simulation is larger to the tests. This comes from the fact that the friction between the wire rings held together by small clamps and the cross section of ring sets does not remain circular. Overall, the force-displacement curves from the theoretical calculation and numerical simulation coincide well with the test data, and the ring sets could be simplified by the beam elements using the equivalent cross section radius.

In the ring nets, one ring set is connected by other four ring sets. Considering the connection between the ring nets, the vaulted structure and other components, and the performance observed in the experiment, the dislocation and fracture of the ring sets would almost not to happen in the ring nets, and a new simplified 2D model for the ring nets is presented in this paper. In the model, one ring set is assumed to be tangential with the other four ring sets, and the two nodes are built on the tangent point belonging to two ring sets with the same location and are coupled with translation degrees of freedom. Therefore, only the tensile load could be transmitted between the ring sets (Figure 12).

3.2. Modeling the Mechanical Behavior of the Wire Meshes. In the wire mesh (Figure 13(a)), the diamond meshes are formed by the two or several wires which are woven together. The details and components of the wire meshes are seen in the Figure 13(b), and in the wire meshes, the single wire diameter d is 3.0 mm, the incircle diameter of mesh D is 65 mm, the angle of mesh ε is 49 degrees, and the mesh size x and y is 83 mm and 143 mm each. The total height of mesh h_{tot} is 12.5 mm, and the clearance of mesh h1 is 6.5 mm.

Quasistatic tensile tests have been implemented on the wire meshes, and the junctions of adjacent diamonds are fractured firstly (Figure 14). That is because in the wire meshes, the junctions of adjacent diamonds can only transmit tensile load, but the single wire in the junction is endured with bending moment and axial force. In the tensile experiments, the average tensile load obtained by the tests is 21.98 kN.

Some research studies have focused on the wire meshes with loose connections. With the FEM methods, the chain-to

(a) (b)

Figure 8: Quasistatic tensile tests on a ring set.

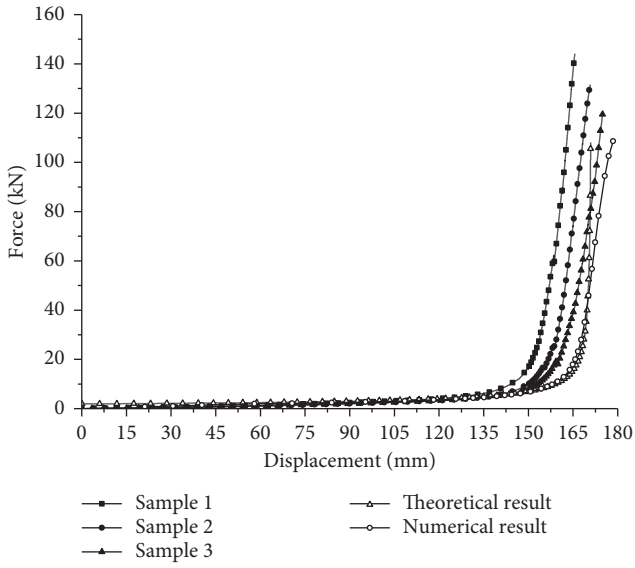

Figure 9: The force-displacement curves for ring nets.

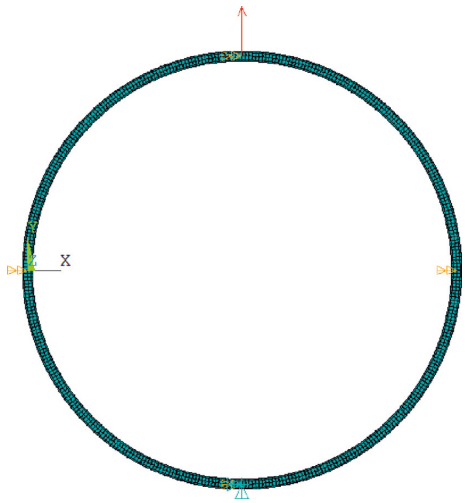

Figure 10: The model of the ring set under the force on two sides.

chain contact is considered to describe mechanical behavior of the wire meshes, and the numerical approach is relied on the general contact algorithm of Abaqus/explicit [15]. With the DEM methods, the hexagonal wire meshes are described with a stochastically distorted contact model [16–18]. In the flexible rock shed, the wire meshes have been stretched after the installation, and in the full-scale experiment, the wire meshes are not fractured or loosened. Take into account the above two reasons, the simplified 2D numerical model for the wire meshes are established as follows.

In the model, the two nodes are built on the junctions of the diamonds belonging to two diamonds with the same location and are coupled with translation degrees of freedom (Figure 15), so they can only transmit the tensile load between the two diamonds, and in each diamond, the single wire bears bending moments and axial forces. Numerical simulation of the tensile tests for the wire meshes is carried out, and the element for discretizing the wire meshes, the constitutive model for the material, and the numerical methods used are just the same as analyzing the ring sets which are presented in the part 3.1.

In Figure 16, the numerical simulation results are also shown and compared with the experimental data. The maximum force obtained by the numerical simulation is 18.50 kN, that is, a little lower than the experimental average result. The maximum displacement obtained by the numerical simulation is 47.783 mm and much lower than the experimental results. That is because on the sides, the wire meshes are connected by the wire rings (Figure 14) which would be slipped and deformed. Overall, the model can rationally express the mechanical properties of the wire meshes.

3.3. Elements and Materials for Ring Nets, Wire Meshes, and Vaulted Structure. Since arched beams, columns, longitudinal supports, shearing supports, and net-hanging brackets in the flexible rock shed are thin-walled structures, the element type "Shell163" which is a 4-node shell element with both bending and membrane capabilities is used to discretize them. Three-dimensional spar element "Link160" which carries axial force only is employed to model the longitudinal support cables, the hoop support cables, and the intersection cables. The three-dimensional spar element "Beam160" is employed to model the ring nets and wire meshes. For the discretization of rock block, element "Solid164" is used, which is defined by eight nodes.

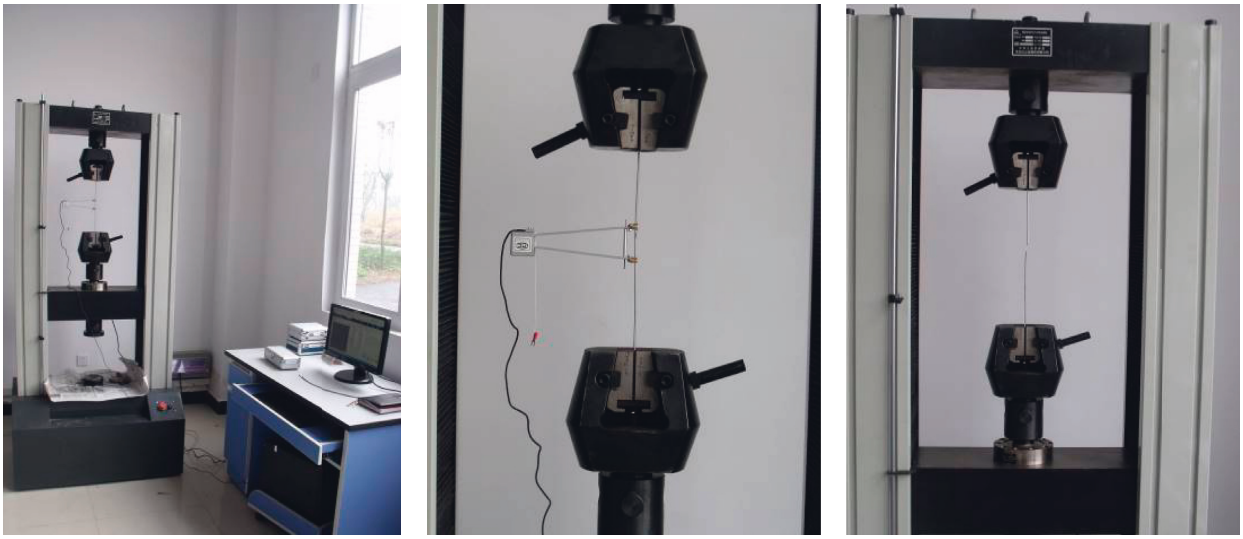

(a) (b) (c)

Figure 11: The tensile tests on the single wire.

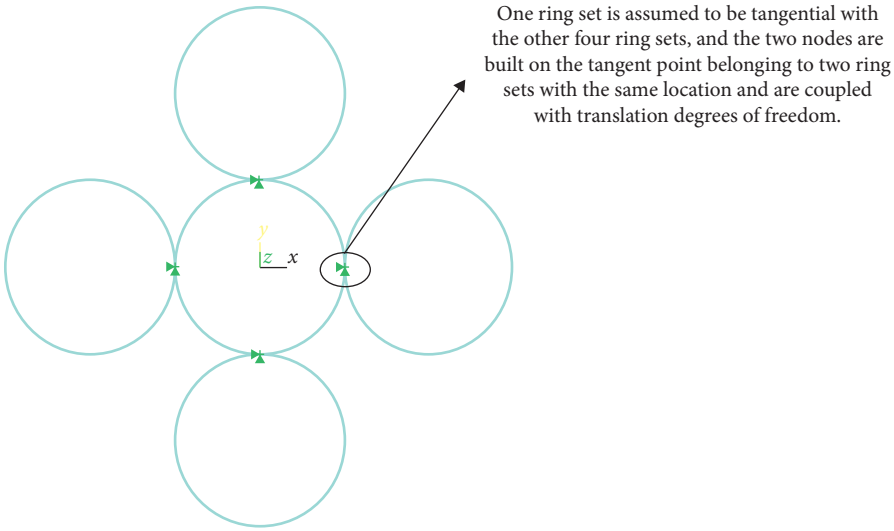

Figure 12: The model of the ring nets composed with ring sets.

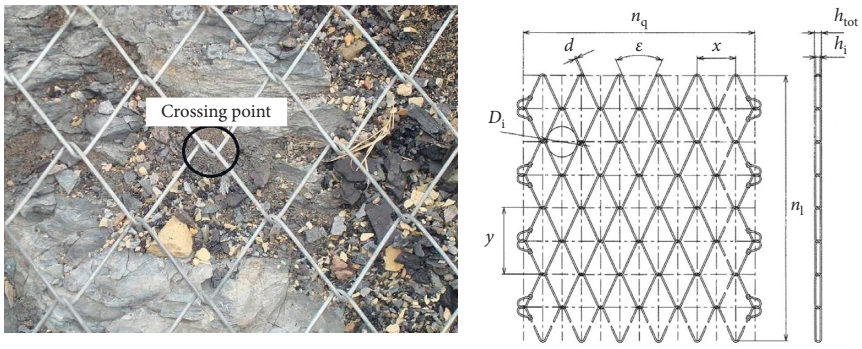

(a) (b)

Figure 13: (a) The wire meshes with diamond patterns; (b) the details and components of the wire meshes.

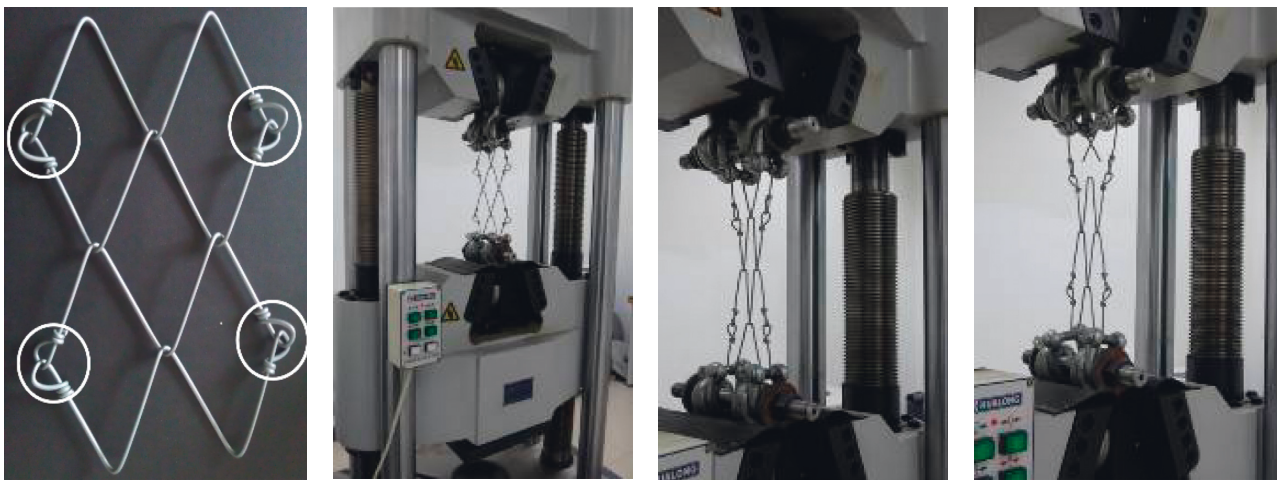

(a) (b) (c) (d)

Figure 14: Quasistatic tensile tests on the wire meshes.

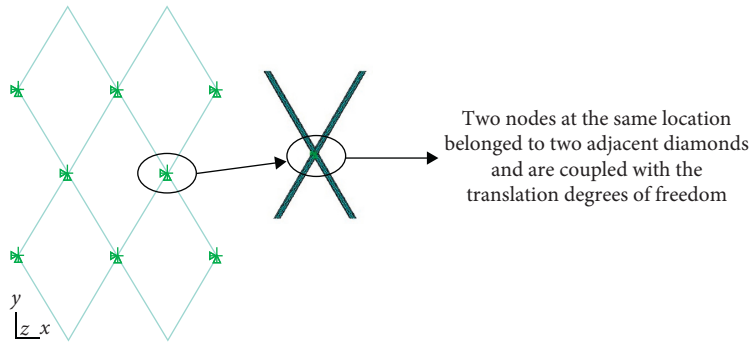

Figure 15: The model of the wire meshes.

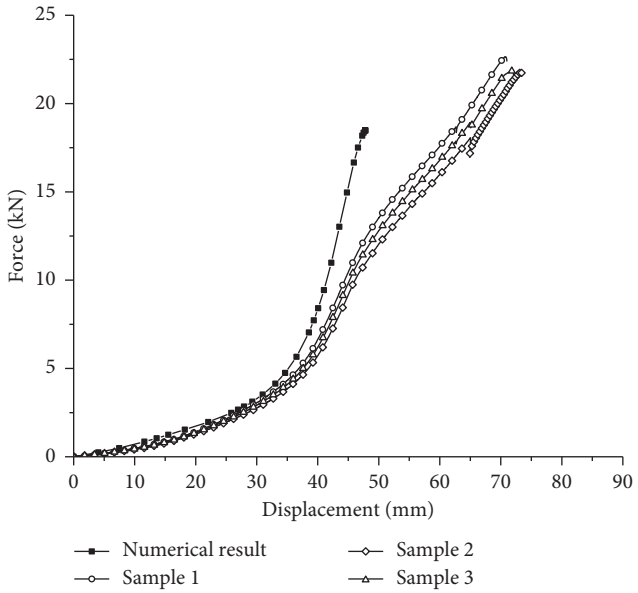

Figure 16: The force-displacement curves for wire meshes.

For the support cables, the ring nets, the wire meshes, and the vaulted structure, failure should be considered. For the sake of simplicity, bilinear isotropic hardening material model (Figure 17) is selected to describe the material behavior of the steel, the cable, and the steel wire used in the flexible rock shed. As cables have strand behavior and do not present a constant elastic modulus, a reduced elastic modulus E and the tangent modulus $E_{\tan}$ are assumed. The material of the steel for the vaulted structure, the steel wire for the ring nets, and the wire meshes are considered as elastic perfectly plastic material. The rock block is neither split nor fragmented in the test and could be defined as rigid bodies. The variation of strain rate in the material would produce significant influence on the hardening of the elastic-plastic material. Among various phenomenological rate-dependent constitutive equations for engineering materials, the Cowper-Symonds relation has been most popularly employed in structural impact problems. This relation represents a rigid, perfectly plastic material with dynamic yield or flow stress that depends on strain rate. Thus, the ratio of dynamic yield stress Y^d to static yield stress Y is

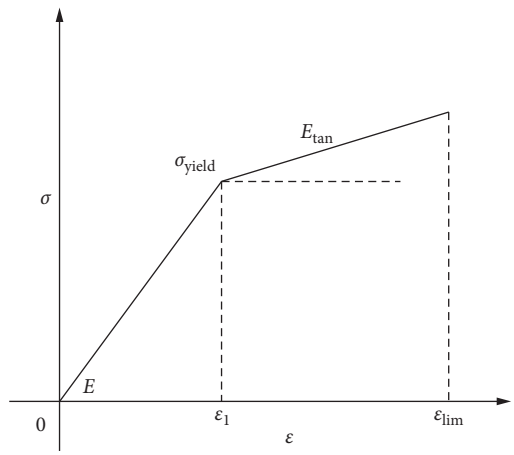

Figure 17: Bilinear isotropic hardening material model.

$$\frac{Y^d}{Y} = 1 + \left(\frac{\dot{\varepsilon}}{C}\right)^{1/P}, \tag{10}$$

where C and P are material constants. Actually, C represents a characteristic strain rate, at which $Y^d = 2Y$, while the material constant P is a measure of the rate sensitivity of material. Therefore, a Cowper-Symonds model is used to take into account the plastic strain rate for the materials, and the values of C and P are set to 40 and 5 each. The material parameters of numerical simulation are listed in Table 2.

The equivalent diameter of cables is obtained by the experiments with inverse analysis [5]. The equivalent diameter of the hoop, intersection, and longitudinal support cables is 16 mm, and their effective cross-sectional area is about 90.96 mm^2. The equivalent diameter of the horizontal cable is 18 mm with an effective cross-sectional area of about 115.25 mm^2.

3.4. Boundary Conditions. For computational efficiency, the following simplifications on connection are introduced into the numerical model:

(1) Hoop support cables, longitudinal support cables, and intersection support cables pass through the upper connection location of the net-hanging bracket (Figure 18). Therefore, the intersection point of hoop, intersection, and longitudinal support cables is assumed as one node, which is coupling with the other two nodes' symmetric distribution on the two sides of the upper location of the net-hanging bracket. These coupled nodes are forced to move with same displacements in order that the support cables and the net-hanging bracket could work together which means the load can transfer among them.

(2) During the impacting process, only one gusset plant was failed (Figure 19), and the local welding spot was broken off after the steel-vaulted structure stopped rebounding. Therefore, stiffened plates and gusset plates are considered to directly connect to arched beam and columns without damage, and the welding failure is neglected.

(3) The ring nets and the wire meshes are connected to the hoop support cables by sewing cables. As no fracture or looseness is observed during the experiment, the ring nets and wire meshes could be assumed to directly connect to the hoop support cables.

Table 2: Material parameters of the numerical model.

Parameter	Steel	Steel wire	Cable	Rockfall
Elastic modules (E, MPa)	2.10e^5	1.77e^5	1.7e^5	3.0e^4
Tangent modulus (E_{tan}, MPa)	0	0	1.7e^4	0
Mean Poisson ratio	0.3	0.3	0.3	0.3
Density (kg/m^3)	7850	7850	7850	2500
Yield stress (σ_{yield}, MPa)	500	1770	1020	—
Limited strain (ε_{lim}, MPa)	0.15	0.03	0.05	—

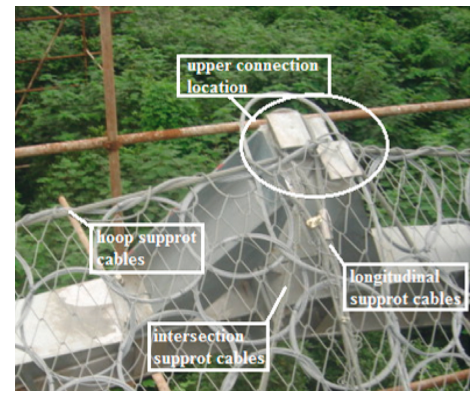

Figure 18: Hoop support cables, longitudinal support cables, and intersection support cables pass through the upper connection location of net-hanging bracket.

The bottoms of columns and the hoop support cables connected to the cable anchors are fixed to the ground. The block is located at the midspan of the structure nearly contacting to the flexible nets with an impacting speed of about 25 m/s and a gravitational acceleration of 9.8 m/s^2 (Figure 20).

4. Numerical Simulation Results

The impact of the rock block on the flexible rock shed is simulated by using commercial FE software package LS-DYNA. Results obtained from the numerical simulation are compared with experimental data to assess the reliability and accuracy of the model in predicting the dynamic behavior of the structure. In particular, the elapsed time, the deformation of the flexible nets and the rock shed, the peak load on the cable anchor and the horizontal cable, and the maximum and minimum principal strain-time curves of the steel-vaulted structure are discussed.

Table 3 shows results about the elapsed time, the deformation of the flexible nets, and the peak load on the cable

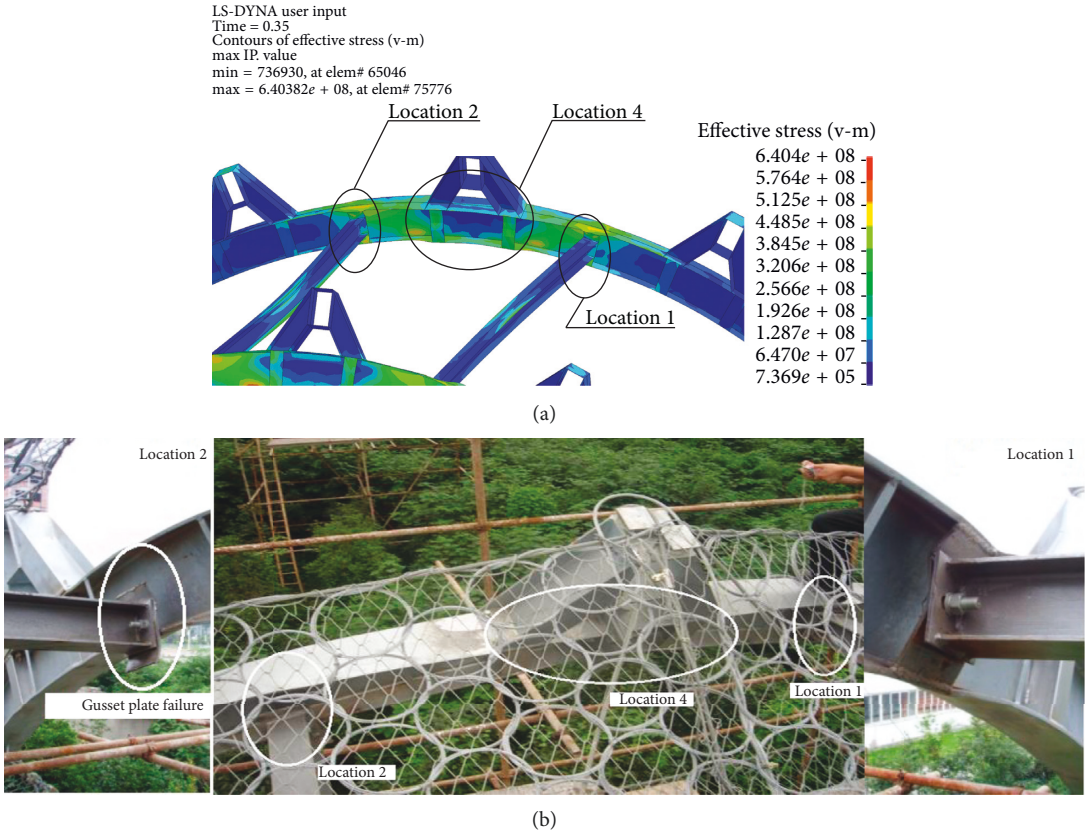

Figure 19: The deformation of the structure at the locations 1, 2, and 4 when block flies off one side of rock shed (numerical simulation and experiment). (a) Numerical simulation and (b) experiment.

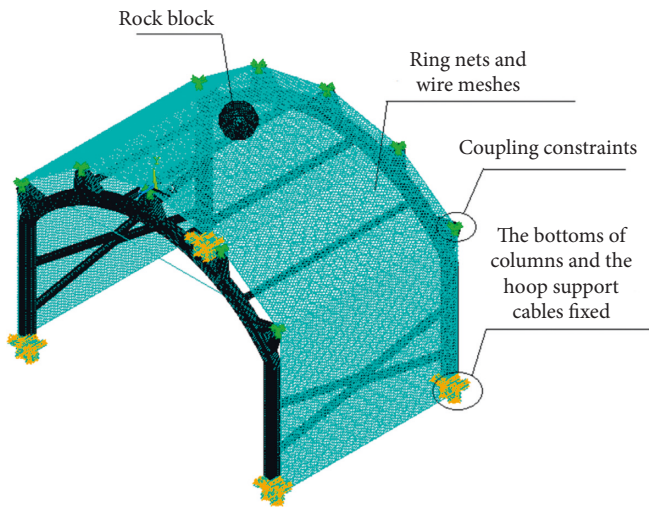

Figure 20: The numerical simulation model with boundary conditions.

Table 3: Comparison between experimental and numerical results.

Item		Experiment	Numerical simulation	Error (%)
Block reaching to the lowest point	Deformation of flexible nets (m)	2.310	1.976	14.5
	Elapse time (s)	0.143	0.119	15.7
Structure stopping rebounding	Deformation of flexible nets (m)	1.780	1.399	21.4
	Elapse time (s)	0.227	0.182	19.8
Peak force (kN)	Horizontal cable	29.5	36.2	22.7
	Cable anchor	21.4	17.6	17.8

anchor and the horizontal cable. As can be seen in Table 3, the two critical deformations of the flexible nets obtained by the numerical simulation are 1.976 m and 1.339 m, corresponding to two critical elapsed times of 0.119 s and 0.182 s, respectively. They all correspond to experimental results given below. This is partially because the ring nets and the wire meshes are loosely connected to the steel-vaulted structure which is not accurately accounted for in the finite element model. The peak forces on the cables obtained by the numerical simulation coincide with the experimental data closely.

Figure 21 compares the experimental and numerical response of the rock shed at three key point frames. The predicted deformed shapes of the prototype are almost the same as those in the corresponding video camera frames. The rock shed's foundational impacting process could be successfully replicated by the presented model.

The maximum and minimum principal strain versus time curves at the pasted location T0, T1-1, and T1-2 could be described through experimental data along three directions obtained by the rosettes at T0, T1-1, and T1-2. Figure 22 shows the maximum and minimum principal strain versus time curves obtained by the experimental data (thin line), as well as the corresponding numerical simulation curves (bold line). As can be seen in Figure 22, the general trend of the numerical simulation matches well with the test. The discrepancy can be partially attributed to the approximation on the connection of the net-hanging bracket, the support cables, and the flexible nets and the difficulty in considering the joints between the arched beams and the columns in the finite element model.

Nevertheless, the numerical simulation results are in fairly good agreement with the experimental data. The presented numerical model is reliable in predicting the dynamic behavior of the whole flexible rock shed under impact.

5. Mechanical Analysis and Improving the Design

The numerical model is employed to investigate the energy absorbed by each component of the rock shed. The energy absorbed by each component reaches its maximum when the energy of the block approaches to 0. The energy absorptions of the components at this moment are recorded in Table 4. As can be seen in Table 4, the energy absorbed by the vaulted structure is the largest, accounting for 76.34% of the total energy; the energy absorbed by the wire meshes comes to the second, accounting for 6.72%, and then the energy absorbed by the ring nets accounts for 5.58%. The energy absorbed by the support cables is negligible, accounting for only about 3.13%. The vaulted structure absorbs most of the energy, thus resulting in serious deformation of the arched beams and net-hanging brackets. It is necessary to increase lateral torsional resistance of the steel-vaulted structure and to reduce the deformation during energy absorption.

For increasing the lateral torsional resistance of the steel-vaulted structure, a simple method is to increase the height, width, and thickness of the components in the steel-vaulted structure. However, this method is not sufficiently economic and applicable. Another method is to improve the connections between components, by reinforcing the weak part and reallocating the energy absorption.

To more reasonably reallocate energy absorption and to make the ring nets and wire meshes absorb more energy at the required deformation distance, the deformation characteristics of the flexible rock shed subjected to the impact are analyzed. Figures 19 and 23 show the detailed deformation at the location 1–4 of the rock shed under the impact obtained by the test and the numerical simulation. From Figures 19 and 23, the following can be stated:

(1) At locations 1 and 2, the longitudinal supports were welded to the gusset plates which were welded to the top and bottom flanges of the arched beam. The force applied on the gusset plates is complex: including shearing forces, bending moments, and axial forces. As can be seen in Figure 19, the gusset plate was buckled, and the flanges deflected seriously (see location 1 in the Figure 19(b)) or the welding between the gusset plant and the top flange was failure (see location 2 in the Figure 19(b)). The longitudinal supports did not deform much because the welding locations between the gusset plates and the top and bottom flanges were too weak. Therefore, the gusset plants at the location 1 and 2 should be strengthened. Therefore, the longitudinal stiffened plants are added (Figure 24), and the thickness of the gusset plants should be increased to 14 mm (after parameter analysis by numerical simulation).

(2) At locations 3 and 4, the net-hanging brackets caused the distortion of the arched beams. Due to the effect of stiffened plates connected to the net-hanging bracket between the top and the bottom flanges of the arched beam, the top and the bottom flange plates rotated inside simultaneously (Figure 23). Stiffened plates on one side were subjected to compression force and on the other side were subjected to tensile force. Because the external load is greater than the restriction effect of the stiffened plates and the bending capacity differed between stiffened plates and the top and the bottom flanges of the arched beam, serious distortion occurred locally at the arched beam and the stiffened plates. As a result, the capability of stiffened plates to restrict general distortion was deduced, and the flanges and web plant of the arched beams were distorted. In order to increase the capacity of the stiffened plants to restrict the distortion, the width and the thickness of the stiffened plants should be increased to 220 mm and 14 mm (after parameter analysis by numerical simulation) and the longitudinal stiffened plants are also added (Figure 24).

After identifying the weak connections and reinforcing the weak part, the improved design of the rock shed is

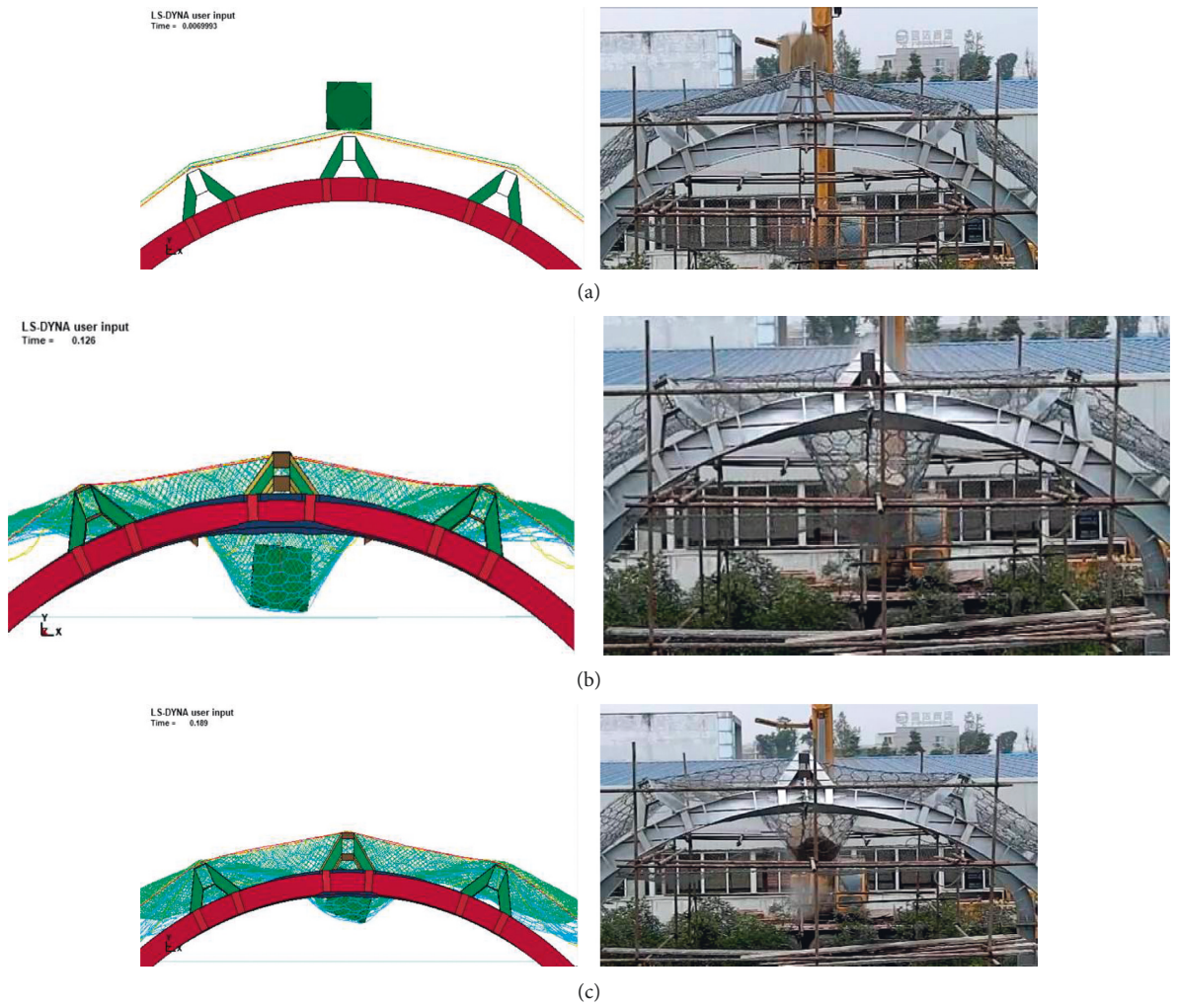

Figure 21: Deformation of the rock shed obtained by the experimental and numerical simulation. (a) Deformation of the rock shed when the block is in contact with the rock shed. (b) Deformation of the rock shed when the block falls in the lowest point. (c) Deformation of the rock shed when the block is still rebounding and steel-vaulted structure stops rebounding.

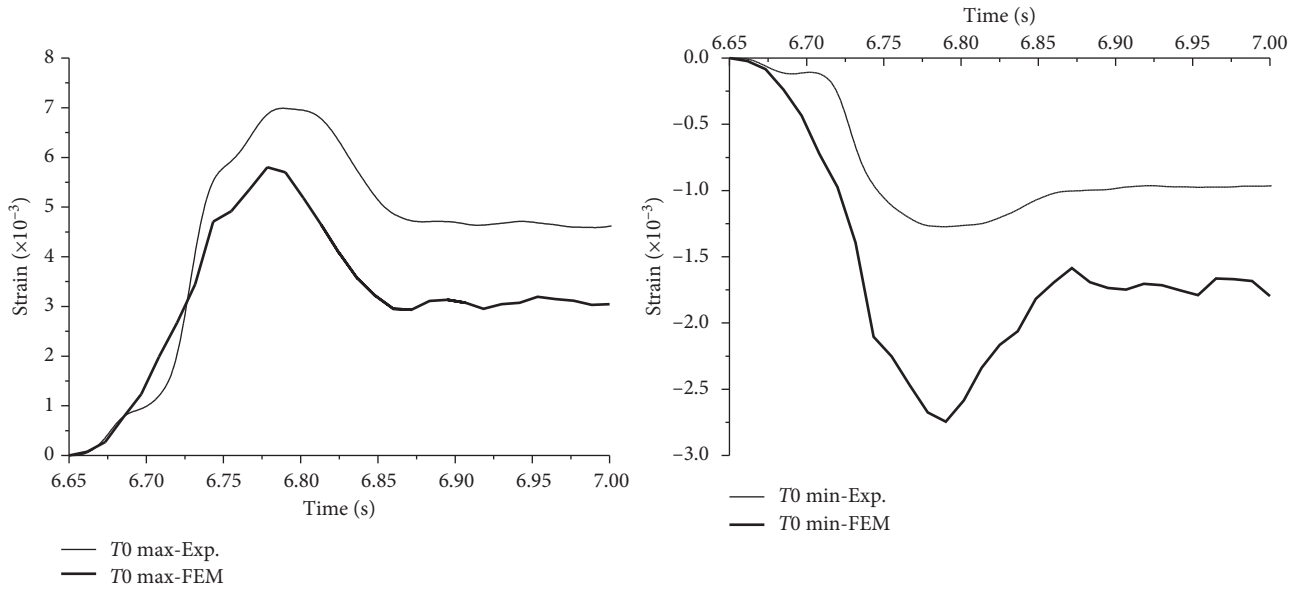

(a)

Figure 22: Continued.

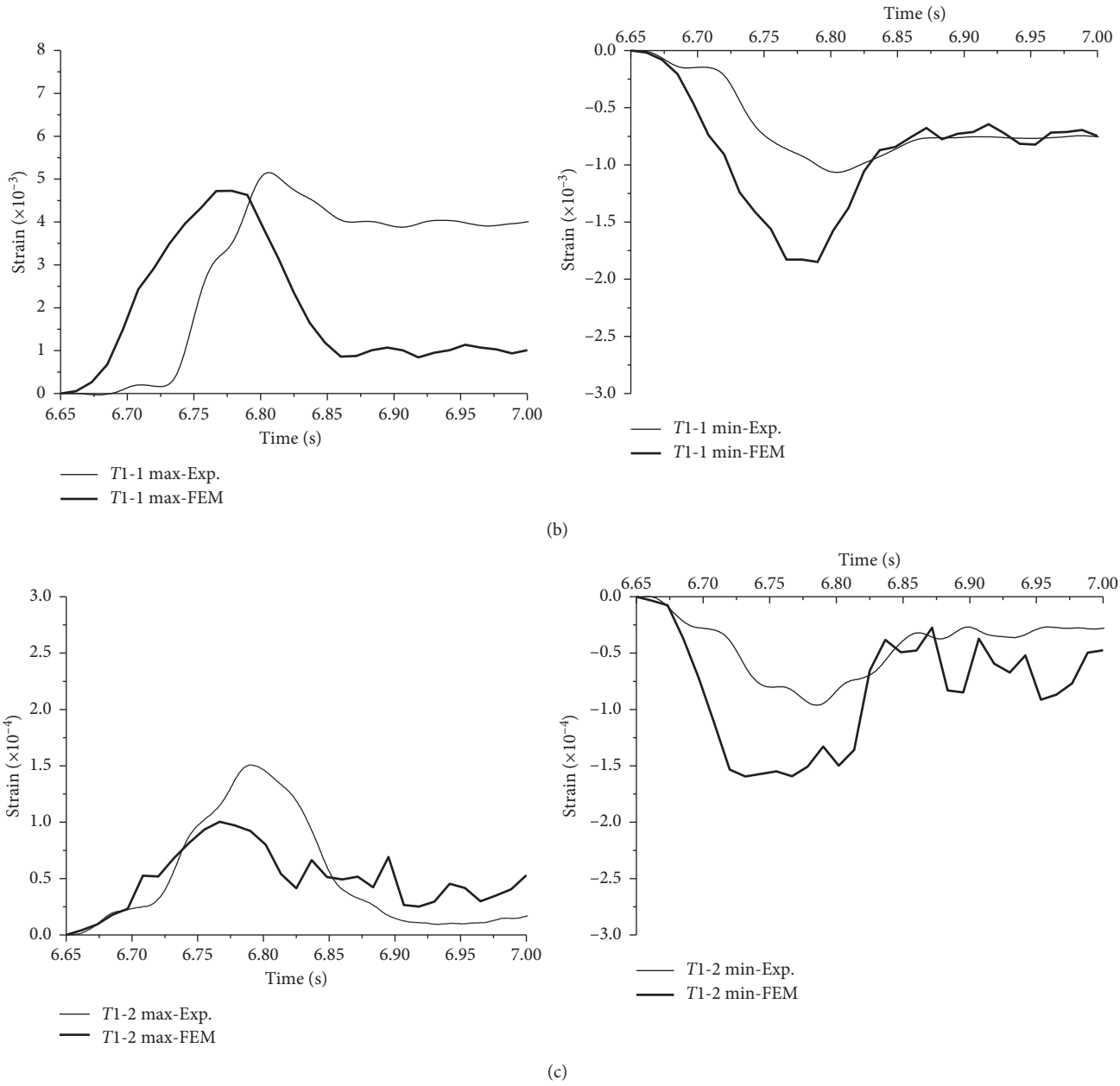

Figure 22: The maximum and minimum principal strain versus time curves. (a) At the T0 location. (b) At the T1-1 location. (c) At the T1-2 location.

Table 4: The maximal energy absorption of the components in the rock shed.

Component	Energy absorption (kJ)	Ratio (%)
Steel-vaulted structure	190.848	76.34
Support cables	7.818	3.13
Ring nets	13.958	5.58
Wire meshes	16.812	6.72
Sliding energy	14.295	5.72
Hourglass energy	1.484	0.59

Note. Sliding energy refers to the energy dissipated due to the friction between block and flexible rock shed.

performed and shown in Figure 24. The next step is to check the behavior of the improved designed rock shed under the same impact as in previous simulation. The results obtained are compared with the original designed rock shed, and the deformation of the structure, the energy absorption by the components, and the maximum deformation of the flexible nets are discussed.

Figures 25 and 26, respectively show the comparison of deformation at location 1–4 between the original and improved designed steel-vaulted structure. As can be seen in Figures 25 and 26, the deformation of the arched beams was much improved, with reduced lateral displacement of net-

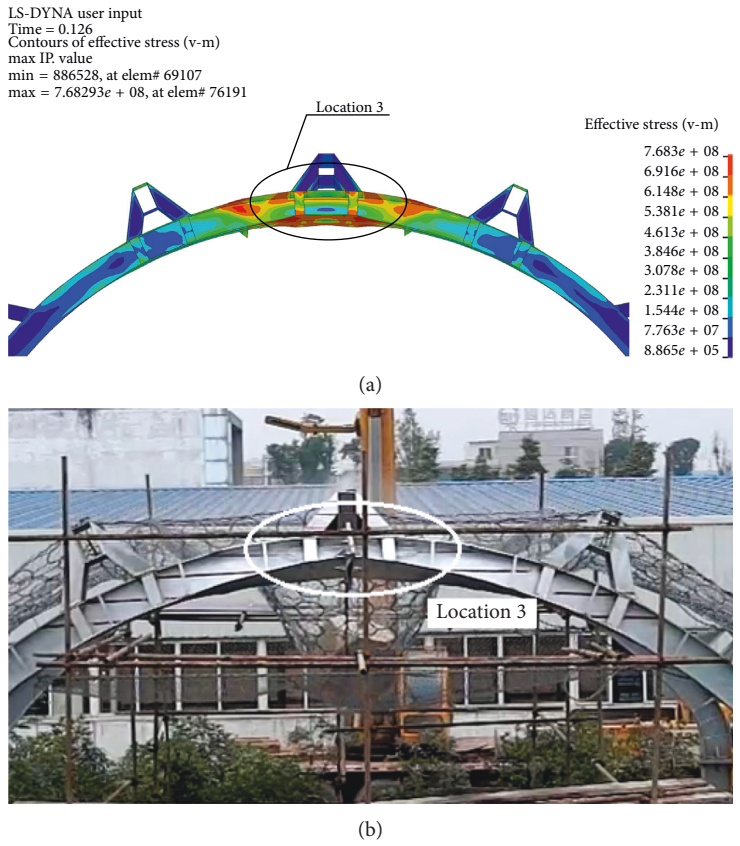

Figure 23: The deformation of the structure at the location 3 when block is down to the lowest point numerical (numerical simulation and experiment). (a) Numerical simulation and (b) experiment.

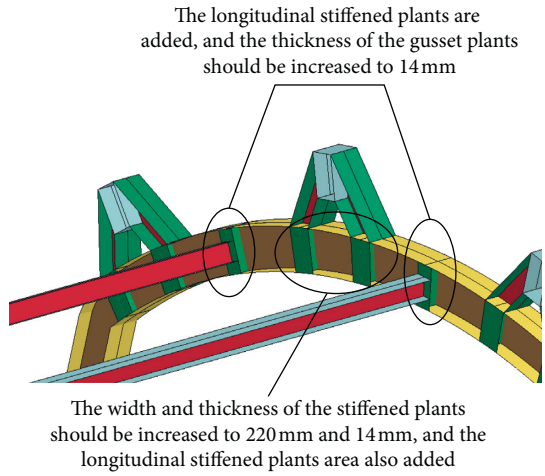

Figure 24: The improved design for the flexible rock shed.

hanging bracket and distortion of arched beam. The steel-vaulted structure can be put into service again with minor maintenance.

The maximum energy absorbed by each component is derived from the simulation and listed in Table 5. As can be seen in Table 5, compared with that in original design, the energy absorption by the steel-vaulted structure is significantly reduced, from 76.34% to 30.19%, whereas the energy absorbed by the ring nets and wire meshes is significantly increased, from 5.58% and 6.72% to 21.59% and 14.97%, respectively. The maximum deformation of the flexible nets is 2.12 m, resulting in a safety distance of 4.880 m which is greater than traffic vehicle height (maximum 4.0 m).

6. Conclusion

(1) Finite element analysis was carried out to simulate the impact test of a new type flexible rock shed for

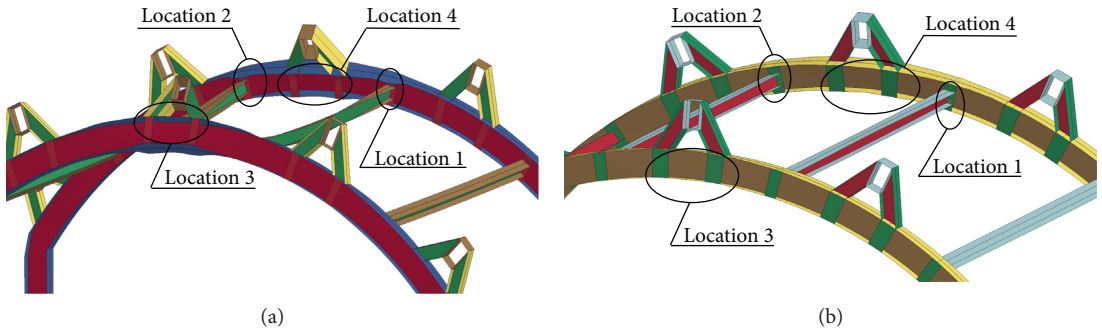

Figure 25: Comparing deformation of the original design (a) and the improved design (b) when the block falls to the lowest point.

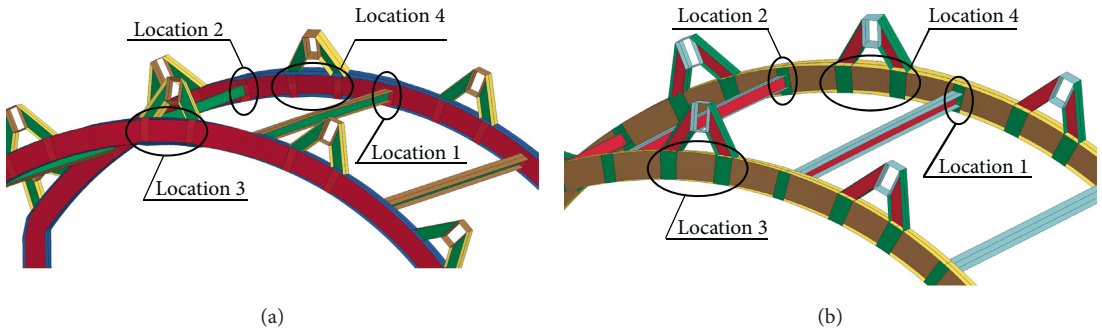

Figure 26: Comparing deformation of the original design (a) and the improved design (b) when the steel-vaulted structure stops rebounding.

Table 5: The maximum energy absorption of the components in the improved designed rock shed.

Component	Energy absorption (kJ)	Ratio (%)
Steel-vaulted structure	75.485	30.19
Support cables	22.889	9.16
Ring nets	53.969	21.59
Wire meshes	37.418	14.97
Sliding energy	40.498	16.12
Hourglass energy	15.688	6.28

Note. Sliding energy refers to the energy dissipated due to the friction between block and flexible rock shed.

the purpose of detailed analysis and improved design. The equivalent radius of the ring set is employed to simplify the ring set model, and a new model for ring nets and wire meshes is presented. Comparison between numerical results and experiment data demonstrates the reliability of the flexible rock shed FE model in predicting the dynamic behavior of the structure. Mechanical analysis and parametric study is then implemented for the improved design of the flexible rock shed. Compared to the original design, the energy absorbed by the steel-vaulted structure is significantly decreased with the ring nets and wire meshes absorbing more energy. Damages on the arched beams are much improved, and the structure can be put into service again with minor maintenance.

(2) However, there are some limiting factors in the case of flexible rock shed according to the rockfall settings and the experimental investigation. The present flexible rock shed can only used for low or about 250 kJ energy rockfall settings. If the structure has experienced rockfall events with half or full energy retention capacity of the structure, the vaulted structure would be deformed much and would require immediate maintenance. Therefore, regular inspection is necessary for this structure. The flexible rock shed cannot be used if the frequency and intensity of rockfall is higher or if the perpetual protection structures are needed considering economical factors.

Data Availability

The data used to support the findings of this study are available from the corresponding author upon request.

Conflicts of Interest

The authors declare that they have no conflicts of interest.

Acknowledgments

This study was funded by the National Natural Science Foundation of China (51408602) and the China Postdoctoral Science Foundation (2017M611815).

References

[1] L. M. Cui, M. Wang, J. H. Sun, and Z. J. Chu, "Theoretical study on the reinforcement capacity of cable nets in active

rockfall protection system," *Engineering Transactions*, vol. 65, pp. 391–401, 2017.

[2] F. Delhomme, M. Mommessin, J. P. Mougin, and P. Perrotin, "Behavior of a structurally dissipating rock-shed: experimental analysis and study of punching effects," *International Journal of Solids and Structures*, vol. 42, no. 14, pp. 4204–4219, 2005.

[3] A. Q. Bhatti and N. Kishi, "Impact response of RC rock-shed girder with sand cushion under falling load," *Nuclear Engineering and Design*, vol. 240, no. 10, pp. 2626–2632, 2010.

[4] A. Volkwein, K. Schellenberg, V. Labiouse et al., "Rockfall characterisation and structural protection—a review," *Natural Hazards and Earth System Sciences*, vol. 11, no. 9, pp. 2617–2651, 2011.

[5] M. Wang, *The engineering application and the design research of the flexible protective technique and the flexible rock shed*, Ph.D. thesis, Logistical Engineering University, Chongqing, China, 2011.

[6] J. P. Mougina, P. Perrotina, M. Mommessina, J. Tonnelob, and A. Agbossoua, "Rock fall impact on reinforced concrete slab: an experimental approach," *International Journal of Impact Engineering*, vol. 31, no. 2, pp. 169–183, 2005.

[7] S. Q. Shi, M. Wang, X. Q. Peng, and Y. K. Yang, "A new-type flexible rock-shed under the impact of rock block: initial experimental insights," *Natural Hazards and Earth System Sciences*, vol. 13, no. 12, pp. 3329–3338, 2013.

[8] A. Volkwein, *Numerische simulation von flexiblen steinschlagschutzsystemen*, Ph.D. thesis, Swiss Federal Institute of Technology, Zürich, Switzerland, 2004.

[9] J. P. Escallón, C. Wendeler, E. Chatzi, and P. Bartelt, "Parameter identification of rockfall protection barrier components through an inverse formulation," *Engineering Structures*, vol. 77, pp. 1–16, 2014.

[10] F. Nicot, B. Cambou, and G. Mazzoleni, "Design of rockfall restraining nets from a discrete element modelling," *Rock Mechanics and Rock Engineering*, vol. 34, no. 2, pp. 99–118, 2001.

[11] C. Gentilini, L. Govoni, S. de Miranda, G. Gottardi, and F. Ubertini, "Three-dimensional numerical modelling of falling rock protection barriers," *Computers and Geotechnics*, vol. 44, pp. 58–72, 2012.

[12] C. Gentilini, G. Gottardi, L. Govoni, A. Mentani, and F. Ubertini, "Design of falling rock protection barriers using numerical models," *Engineering Structures*, vol. 50, pp. 96–106, 2013.

[13] J. B. Coulibaly, M. A. Chanut, S. Lambert, and F. nicot, "Nonlinear discrete mechanical model of steel rings," *Journal of Engineering Mechanics*, vol. 143, no. 9, article 04017087, 2017.

[14] G. X. Lu and T. X. Yu, *Energy Absorption of Structures and Materials*, Woodhead Publishing, Cambridge, UK, 2006.

[15] J. P. Escallón, V. Boetticher, C. Wendeler, E. Chatzi, and P. Bartelt, "Mechanics of chain-link wire nets with loose connections," *Engineering Structures*, vol. 101, pp. 68–87, 2015.

[16] D. Bertrand, F. Nicot, P. Gotteland, and S. Lambert, "Discrete element method (DEM) numerical modeling of double-twisted hexagonal mesh," *Canadian Geotechnical Journal*, vol. 45, no. 8, pp. 1104–1117, 2008.

[17] K. Thoeni, C. Lambert, A. Giacomini, and S. W. Sloan, "Discrete modelling of hexagonal wire meshes with a stochastically distorted contact model," *Computers and Geotechnics*, vol. 49, pp. 158–169, 2013.

[18] K. Thoeni, A. Giacomini, C. Lambert, S. W. Sloan, and J. P. Carter, "A 3D discrete element modelling approach for rockfall analysis with drapery systems," *International Journal of Rock Mechanics and Mining Sciences*, vol. 68, pp. 107–119, 2014.